ACS APPLIED MATERIALS & INTERFACES

Research Article

www.acsami.org

Solvothermal Synthesis of Tetrahedrite: Speeding Up the Process of Thermoelectric Material Generation

Derak J. James,[†,§] Xu Lu,[‡,§] Donald T. Morelli,[‡] and Stephanie L. Brock*[,†]

[†]Department of Chemistry, Wayne State University, Detroit, Michigan 48201, United States

[‡]Department of Chemical Engineering and Materials Science, Michigan State University, East Lansing, Michigan 48824, United States

Supporting Information

ABSTRACT: Derivatives of synthetic tetrahedrite, $Cu_{12}Sb_4S_{13}$, are receiving increasing attention in the thermoelectric community due to their exploitation of plentiful, relatively nontoxic elements, combined with a thermoelectric performance that rivals that of PbTe-based compounds. However, traditional synthetic methods require weeks of annealing at high temperatures (450−600 °C) and periodic regrinding of the samples. Here we report a solvothermal method to produce tetrahedrite that requires only 1 day of heating at a relatively low temperature (155 °C). This allows preparation of multiple samples at once and is potentially scalable. The solvothermal material described herein demonstrates a dimensionless figure of merit (ZT) vs temperature curve comparable to that of solid-state tetrahedrite, achieving the same ZT of 0.63 at ∼720 K. As with the materials from solid-state synthesis, products from this rapid solvothermal synthesis can be improved by mixing in a 1:1 molar ratio with the Zn-containing natural mineral, tennantite, to achieve 0.9 mol equiv of Zn. This leads to a 36% increase in ZT at ∼720 K for solvothermal tetrahedrite, to 0.85.

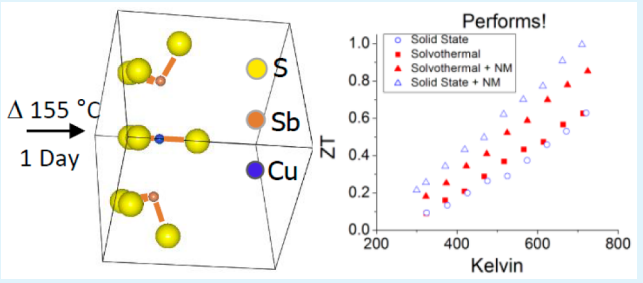

KEYWORDS: *tennantite, mineral, zinc doping, ZT, $Cu_{12}Sb_4S_{13}$*

1. INTRODUCTION

Thermoelectric materials offer an environmentally friendly way to increase energy efficiency by generating electricity from the plentiful waste heat of manufacturing processes and combustion.[1] Conserving energy through efficiency carries the twin benefits of not only decreasing pollution from coal but also lowering production costs of manufactured goods, thus allowing a higher standard of living through cleaner air while saving businesses money. However, available thermoelectric materials are impractical for large-scale production or widespread use because of the synthetic complexity, the lengthy time required for preparation,[2−9] the incorporation of toxic or rare elements,[10−18] or the low efficiency as rated by the dimensionless figure of merit, $ZT = T\alpha^2/(\rho\kappa_{tot})$.[1] The parameters comprising ZT (Seebeck coefficient, α; electrical resistivity, ρ; and total thermal conductivity, κ_{tot}, which itself is the sum of electronic charge carrier (κ_C) and lattice (κ_L) contributions) couple unfavorably, making the realization of large ZT values, a considerable challenge to materials scientists. PbTe is a traditional thermoelectric material for high-temperature use, exhibiting a ZT of ∼1 at 650 K. Attempts to make "greener" thermoelectric materials have focused on copper-sulfides and selenides, particularly those adopting the chalcopyrite (zinc-blende-based) structure type. However, doped $CuInSe_2$ and $CuInS_2$ exhibit relatively low ZT values even up to 550 K,[19,20] whereas the more promising nanostructured $CuAgSe_2$ reaches a maximum ZT value of 0.55 at 700 K.[10,21]

Tetrahedrite,[2,3] $Cu_{12}Sb_4S_{13}$, is emerging as a promising phase for thermoelectrics. It exhibits an intrinsically low lattice thermal conductivity (κ_L = 0.4W m^{-1} K^{-1} at 700 K) due to unique features in its crystal structure (Figure 1). Specifically, a trigonal planar Cu^+ ion bound by three S^{2-} ions is capped above and below by Sb^{3+} ions, each possessing a lone pair and forming a trigonal pyramid with three different S^{2-} ions. The anharmonic vibration of these Cu ions vertical to the triangle plane results in dynamic interactions with the lone pairs on the Sb ions above and below.[22] This results in a trigonal bipyramidal Cu^+ that acts as a rattler in a cage. The changing vibration frequency with cell volume leads to a high Grüneisen parameter resulting in low κ_L values due to destructive interference of the phonons.[23] At the same time, the defect zinc-blende lattice ensures a good "crystalline" pathway for electron transport.

The role of lone pairs contributed by Sb^{3+} may be further explored by comparison of tetrahedrite crystal structures formed by $Cu_{12}Sb_2Te_2S_{13}$ (κ_L = 0.7 W m^{-1} K^{-1}) and $Cu_{10}Te_4S_{13}$ (κ_L = 1.4 W m^{-1} K^{-1}).[24] The latter compound possesses random copper vacancies in the tetrahedrite structure, which fail to lower the κ_L value. The low κ_L value of $Cu_{12}Sb_2Te_2S_{13}$ is due to a unique abundance of low energy (∼3 meV) vibrational modes not present in $Cu_{10}Te_4S_{13}$, and

Received: August 3, 2015
Accepted: October 6, 2015
Published: October 19, 2015

DOI: 10.1021/acsami.5b07141
ACS Appl. Mater. Interfaces 2015, 7, 23623−23632

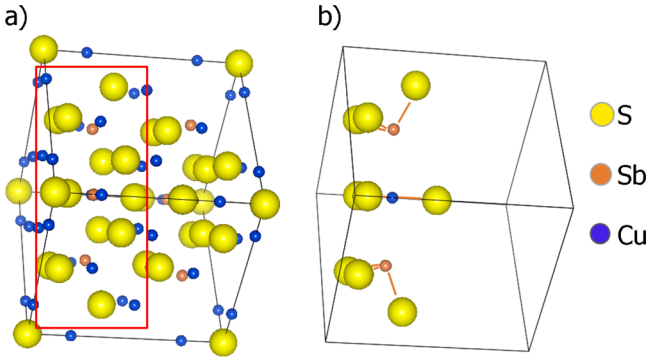

Figure 1. Unit cell (a) of tetrahedrite, Inorganic Crystal Structure Database code 41753, projected parallel to a triangular plane formed by a Cu atom (blue) with three S atoms (yellow) is displayed. A rectangle is added to emphasize a region of the cell containing an arrangement of two trigonal pyramidal Sb atoms (brown) above and below the trigonal planar Cu. The unit cell is displayed again in the same orientation (b) showing only the two trigonal pyramidal Sb ions and the trigonal planar Cu, ion. The unit cell is rendered by the Visualization for Electronic and Structural Analysis program.[34]

Raman spectroscopy measurements associate these with out-of-plane vibrations of the trigonal planar copper. These results corroborate an increased out-of-plane displacement of the trigonal planar copper in $Cu_{12}Sb_2Te_2S_{13}$ compared to $Cu_{10}Te_4S_{13}$. This indicates that the $5s^2$ lone pair from antimony interacts with copper while that of tellurium is truly inert. Bouyrie et al. suggest that, rather than a bond being formed, the displacement of the trigonal planar copper results in a dipole that interacts with the dipole formed by the stereochemically active (from partial sp^3 hybridization) lone pair on Sb^{3+}. This results in the low energy vibrational modes that interfere with acoustical phonons, scattering them for decreased κ_L. Similar low energy (4 meV) vibrational modes were assigned to the trigonal planar copper in pure tetrahedrite, $Cu_{12}Sb_4S_{13}$.[22]

The present work focuses on quickly and efficiently producing $Cu_{12}Sb_4S_{13}$ in a manner adaptable to industrial production. The electronic properties are then optimized by mixing with the natural mineral form, tennantite ($Cu_{10.0}Zn_{1.8}Fe_{0.2}As_{2.7}Sb_{1.3}S_{13}$), to dope by substitution of zinc for copper to maximize ZT. The pure tetrahedrite, $Cu_{12}Sb_4S_{13}$, is *p*-type with two available energy states in the valence band above the Fermi Level that electrons can easily be excited into, resulting in metallic character.[2,25,26] The bandgap is between 1.2 eV for bulk and up to 1.7 eV for nanocrystals and can be modified by doping with transition metals.[2,25−27] For instance, bulk tetrahedrite doped with Zn^{2+} or Mn^{2+} has demonstrated bandgaps of 1.8 eV.[28] Substitution of the Cu^{2+} ions (comprising 1/6th of the copper ions in the structure, with the balance being monovalent) by Zn^{2+} is proposed to raise α and ρ by raising the Fermi level toward the top of the valence band by adding one electron per Zn^{2+}.[2,3] This substitutional doping has been achieved by ball-milling the natural mineral, which contains enough Zn to render it an electronic insulator, with synthetic tetrahedrite prepared by high-temperature solid-state methods (solid-state tetrahedrite) to form a solid solution that is optimally doped, yielding a ZT ∼ 1 at 700 K.[3]

Although tennantite also serves as a source of iron or arsenic, arsenic incorporation has not been discussed as playing a role in tuning electronic properties in previous works.[2,3] However, mixing iron-rich tennantite ($Cu_{10.5}Fe_{1.5}As_{3.6}Sb_{0.4}S_{13}$) with synthetic tetrahedrite has been found to increase ZT by tuning electronic properties to an optimum doping level of 0.38 mol equiv of iron (vs 0.9 mol of Zn). Nevertheless, the ZT is lower (0.8 at ∼700 K) than that achieved by mixing tetrahedrite with the zinc-rich tennantite.[3] The iron present from mixing zinc-rich tennantite ($Cu_{10.0}Zn_{1.8}Fe_{0.2}As_{2.7}Sb_{1.3}S_{13}$) in a 1:1 mol ratio with tetrahedrite would be quite small at 0.1 mol equiv. At this amount, the iron would be Fe^{3+} and would contribute two extra electrons to the valence band per iron, raising the Fermi Level similarly to zinc.[2,29] However, the Fe^{3+} also results in impurity bands above the Fermi Level in Fe-doped tetrahedrite.[25,29] The impurity bands are formed due to the magnetic moment of Fe^{3+} from the d^5 electron configuration. The magnetic moment results in a splitting of available energy states in the valence band. The electrons can either be aligned with the majority of spins from unpaired electrons, lowering the energy, or be opposed to them, raising the energy. This results in a majority-spin band below the Fermi Level and a minority-spin band above it. The addition of Zn-doping raises the Fermi Level, and the minority-spin band provides extra energy states to be filled by the added electrons from Zn-doping. Therefore, the Fe-doping could increase the amount of zinc that can be incorporated before the material becomes insulating. As a result, the maximum ZT ∼ 1 was achieved for x = 0.95 ($Cu_{12-x}M_xSb_4S_{13}$, with M = Fe, Zn) using zinc-rich tennantite as the dopant source.[3] This is significantly more zinc than the x = 0.5 required for optimal Zn-doping (ZT ∼ 1) of solid-state tetrahedrite ($Cu_{12-x}Zn_xSb_4S_{13}$) in the absence of iron.[2]

In addition to doping tetrahedrite with zinc by ball-milling with the natural mineral tennantite, zinc can also be incorporated by in situ doping during solid-state synthesis to optimize ZT ($Cu_{12-x}Zn_xSb_4S_{13}$, x = 0.5−1.0).[2,25,28,30] This latter method has been used to dope tetrahedrite with a variety of metals including manganese, iron, cobalt, and nickel.[25,28,30−33] The pure element is used as the source of dopant in solid-state syntheses, and is mixed with copper, antimony, and sulfur in the desired stoichiometry to yield the product $Cu_{12-x}M_xSb_4S_{13}$ with M = Zn, Mn, Fe, Co, Ni, or Zn.

The combination of a composition that comprises abundant elements, tunable electronics, intrinsically low lattice thermal conductivity, and the ability to dope by forming a solid solution with the naturally occurring mineral has led to several licensed patents for tetrahedrite as a thermoelectric.[35,36] However, there are problems with existing preparations for the synthetic tetrahedrite that need to be addressed if it is to be produced on a large scale (i.e., industrially). Tetrahedrite is currently prepared by high-temperature solid-state synthesis, which requires 3 days in a dedicated tube furnace as reagents are heated slowly to 650 °C and then slowly allowed to cool.[2,3] The product is then ball-milled and annealed for 2 weeks at 450 °C before ball-milling again and hot-pressing into a pellet. Recent work has demonstrated that tetrahedrite can be grown in solution as discrete nanocrystals by hot-injection methods on a small scale (ca. 0.5 mmol copper precursor per reaction) using long chain ligands as capping agents.[37] However, adaptation of these nanocrystals for thermoelectric use would face the dual challenges of small scale production and the need to eliminate the long chain ligands that increase resistivity by orders of magnitude in other thermoelectric systems.[38,39] Moreover, it is doubtful that the benefits of phonon scattering achieved by nanostructuring[40] will be realized in this system because of the inherently low κ_L.

In the present work, we develop and optimize a ligand-less solvothermal route to synthetic tetrahedrite that can be done

DOI: 10.1021/acsami.5b07141
ACS Appl. Mater. Interfaces 2015, 7, 23623−23632

with 1 day of heating at moderate temperature (ca. 150 °C) and allows parallel processing due to the manageable temperature and pressure requirements. Thermoelectric characterization is carried out on the product as well as on a 1:1 molar mixture of the product with natural mineral (tennantite). We show that properties of the solvothermal tetrahedrite are comparable to those produced by solid-state methods and that our product is amenable to doping by mixing with tennantite.

2. MATERIALS AND METHODS

2.1. Materials. Antimony(III) sulfate (99.7%) and copper(II) nitrate hemi(pentahydrate) (98.0−102.0%) were obtained from Aldrich Chemicals. The largest concentrations of impurities in copper(II) nitrate hemi(pentahydrate) are reported to be sulfate, nickel, and sodium (all <0.01%). Thiourea (99% min.) and antimony(III) chloride (99.0% min.) were obtained from Alfa Aesar. Copper(I) chloride (99% purified) was obtained from Acros. Ethylenediamine (anhydrous) was obtained from Fisher Chemical. Ethanol (200 proof) was obtained from Decon Laboratories, Inc., and concentrated sulfuric acid was obtained from EMD Chemicals. The copper(II) nitrate hemi(pentahydrate) was dried in an oven at 105 °C for 2 days to result in basic copper nitrate, $Cu_2(OH)_3NO_3$. The composition of the natural mineral tennantite (designated here as NM) used for mixing was $Cu_{10.0}Zn_{1.8}Fe_{0.2}As_{2.7}Sb_{1.3}S_{13}$. This was purchased as a mineral specimen from Stefano Fine Minerals, Inc., Ann Arbor, Michigan, USA.

2.2. Synthesis and Characterization. *2.2.1. Synthesis of Tetrahedrite: Literature Method.* There is one previous report of a solvothermal synthesis of tetrahedrite, and we used this as a basis of our initial exploration. The literature synthesis[41] is scaled down from the 50 mL vessel size to the 23 mL vessels that we had available. Briefly, 0.2944 g of copper(I) chloride, 0.2261 g of antimony(III) chloride, 0.2452 g of thiourea, and 18.4 mL of ethanol (200 proof) are added to a solvothermal vessel, which is then sealed in a stainless steel bomb and heated at 155 °C for 20 h. After allowing the vessel to cool, the product is filtered and washed three times with deionized water followed by three ethanol washes. Subsequently the product is dried under vacuum at 50 °C.[41] This synthesis is repeated several times, and the products are combined to result in several grams of material for thermoelectric characterization.

2.2.2. Synthesis of Tetrahedrite: Chloride Free with 100% Molar Excess Sulfur Source. Basic copper nitrate ($Cu_2(OH)_3NO_3$, 0.3570g), antimony(III) sulfate (0.2503g), thiourea (0.4904g), and ethylenediamine (18.4 mL) are combined in a 23 mL Teflon vessel. This is heated in a sealed stainless steel bomb in a furnace at 155 °C for 20−24 h before the furnace is turned off and the pressurized vessel is allowed to cool in the open furnace. The product is then isolated by centrifugation and washed once with deionized water, followed by five times with concentrated sulfuric acid, two times with deionized water, and once with ethanol. The product is then dried under vacuum for at least 4 h.

2.2.3. Synthesis of Tetrahedrite: Chloride Free with 300% Molar Excess Sulfur Source. The synthesis is identical to that described above except that thiourea was increased to 0.9808 g, and the isolation was performed by washing with deionized water (with agitation) followed by centrifugation, followed by washing with sulfuric acid (for 1 min, again with agitation) a total of five times, followed by two times with deionized water and once with ethanol. The yield is about 0.25 g per solvothermal vessel (64% of theoretical yield of 0.3922 g), and these were typically prepared in groups of four at a time.

2.2.4. Synthesis of Tetrahedrite: Solid-State Method. For comparison to solvothermal materials, solid-state tetrahedrite was prepared as described in the literature and yielded thermoelectrical properties similar to those previously reported.[2]

2.2.5. Mixing of Tetrahedrite with NM. Tetrahedrite (solvothermally or solid-state prepared) is ground together with the NM to target a 0.9 mol equiv of Zn. These mixtures were then ball-milled at 1060 cycles per minute for 30 min using a stainless steel ball mill set in a SPEX 8000 Series Mixer.

2.2.6. Structural and Chemical Characterization. Structure identification was achieved using a Rigaku SmartLab Powder X-ray Diffractometer. Dry powders were prepared for X-ray diffraction (XRD) by mixing with silicon powder (as an internal standard) and mounting on a zero-background quartz sample holder. Crystalline products were identified by comparison to diffraction patterns in the ICDD Powder Diffraction File (PDF) database. Product compositions were determined by inductively coupled plasma optical emission spectroscopy (ICP-OES) using a Horiba Ultima ICP-OES. Products were prepared for ICP-OES by dissolving a precisely weighed amount (approximately 14 mg) of product in 40 mL of a solution of concentrated nitric acid and hydrochloric acid prepared in a 1:3 ratio by volume. Deionized water is used to dilute this solution to 500 mL in a volumetric flask.

2.2.7. Thermoelectric Characterization. Each sample is hot-pressed at 80 MPa and 430 °C for 30 min to form a 4.5 mm thick disk 10 mm in diameter; the resulting pellets are >95% theoretical density. A diamond saw is then used to remove a slice of the disk for thermal conductivity measurements, and pellets (approximately 3 × 3 × 7 mm) are cut from the remaining disk as rectangular parallelepipeds for thermoelectric characterization. The leftover portions of the disc are further characterized by XRD for insight on the effects of hot-pressing on crystal structure and phase purity.

In the temperature range 80−300 K, standard steady-state techniques are employed on the rectangular parallelepipeds to measure resistivity, Seebeck coefficient, and thermal conductivity from 80−300 K under high vacuum by exploiting a continuous liquid nitrogen flow cryostat. Radiation losses, which can affect the measurement of thermal conductivity using this steady-state technique near room temperature, are determined by measuring the thermal conductivity of a Pyrex glass standard; these losses are then corrected for in the determination of the sample thermal conductivity. Above room temperature, the Seebeck coefficient and electrical resistivity are measured on the same parallelepipeds using an Ulvac ZEM-3 apparatus. To determine the high-temperature thermal conductivity, a disk-shaped specimen (ca. 10 mm diameter by 1 mm thick) is cut from the same pellet. High-temperature thermal diffusivity is then measured on this disk using the laser flash technique (Netzsch LFA457). Adjacent pieces cut from a nearby area of the pellet samples are used for differential scanning calorimetry (Netzsch, DSC200F3) determination of specific heat. All the specific heat data are close to or higher than the Dulong-Petit value of pure $Cu_{12}Sb_4S_{13}$. Thermal conductivity is then calculated from thermal diffusivity (D), room temperature sample density, and specific heat (C_p) by using $\kappa = D \times \text{density} \times C_p$. We estimate uncertainties of 5% in both Seebeck coefficient and electrical resistivity, and an uncertainty of 10% in thermal conductivity.

3. RESULTS AND DISCUSSION

3.1. Synthesis and Characterization of Tetrahedrite: Literature Method. As a starting point to develop a facile and rapid synthesis of tetrahedrite, our initial studies focused on the one (to our knowledge) report of tetrahedrite formation by a solvothermal approach.[41] This method involves reaction of thiourea (as a sulfur source) with chloride salts of Cu^+ and Sb^{3+} in ethanol in a stainless steel bomb under autogenous pressure at 155 °C for 20 h.

Powder XRD data from the product obtained from the literature preparation reveals both famatinite (Cu_3SbS_4) and tetrahedrite ($Cu_{12}Sb_4S_{13}$) phases (Figure 2), as well as additional impurities that could not be identified relative to known phases in the ICDD-PDF database. The composition was determined to be $Cu_{15.8}Sb_{7.8}S_{13}$ by ICP-OES, which is metal-rich in both copper and antimony. Investigation by TEM and EDS revealed the product to be heterogeneous and to incorporate chlorine (Figure 3). The EDS of the region shown in Figure 3a suggests a composition of $Cu_{13.2}Sb_{4.6}S_{13}Cl_{0.8}$, once

DOI: 10.1021/acsami.5b07141
ACS Appl. Mater. Interfaces 2015, 7, 23623−23632

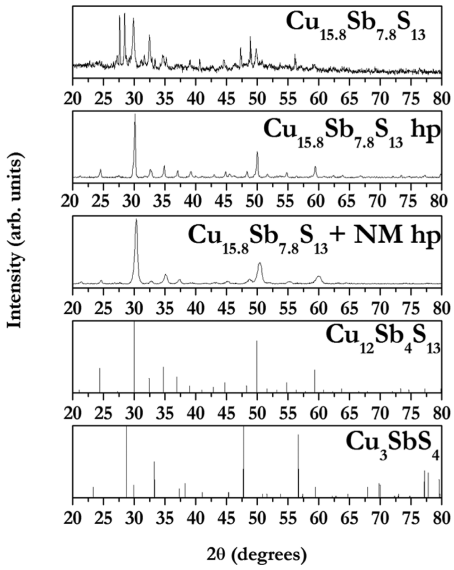

Figure 2. XRD patterns of tetrahedrite synthesized by the reported literature method before ($Cu_{15.8}Sb_{7.8}S_{13}$) and after hot-pressing ($Cu_{15.8}Sb_{7.8}S_{13}$ hp). PDF patterns 42-0561 and 35-0581 are displayed for tetrahedrite ($Cu_{12}Sb_4S_{13}$) and famatinite (Cu_3SbS_4), respectively. The literature-prepared tetrahedrite is ball-milled in a 1:1 molar ratio with the natural mineral tennantite, $Cu_{10}Zn_{1.8}Fe_{0.2}As_{2.7}Sb_{1.3}S_{13}$, and hot-pressed to produce $Cu_{15.8}Sb_{7.8}S_{13}$ + NM hp.

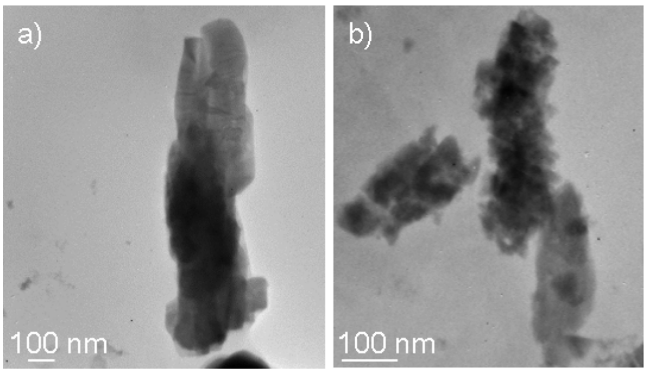

Figure 3. TEM images of different regions of literature-prepared tetrahedrite revealing different compositions by EDS: (a) $Cu_{13.2}Sb_{4.6}S_{13}Cl_{0.8}$ and (b) $Cu_{2.0}S_{0.8}$.

scaled to a sulfur mole contribution of 13. This is less metal-rich than the bulk composition determined by ICP-OES, but there is still more metal than called for by the tetrahedrite formula, and the chlorine contributions cannot be neglected. The EDS of the region imaged in Figure 3b does not show any Sb or Cl, and suggests a composition of $Cu_{2.0}S_{0.8}$, similar to copper(I) sulfide, although this phase is not observed in the XRD pattern, suggesting it is present in small quantities and/or is amorphous.

The literature-prepared tetrahedrite is hot-pressed alone and after mixing with the natural mineral (abbreviated as NM) tennantite ($Cu_{10}Zn_{1.8}Fe_{0.2}As_{2.7}Sb_{1.3}S_{13}$) to achieve a 1:1 molar ratio. After hot-pressing at 430 °C, the material ($Cu_{15.8}Sb_{7.8}S_{13}$ hp) exhibits the XRD pattern of tetrahedrite (Figure 2) with few apparent crystalline impurities, suggesting the hot-pressing process was able to homogenize the mixture. Mixing the literature-prepared tetrahedrite with tennantite by ball-milling and then hot-pressing results in a shift in the tetrahedrite pattern toward higher 2θ, as expected, indicating that zinc is incorporated into the crystal structure as a solid solution (decrease in lattice parameters). Again, no crystalline impurities are revealed.

Relative to the solid-state tetrahedrite, the low-temperature thermoelectric properties of materials produced by the literature method reveal a ca. 20% increased thermopower at room temperature, 97 $\mu V\ K^{-1}$, as shown in Figure 4. This may be due to chloride acting as an electron dopant, filling the valence band holes and pushing the Fermi level toward the band gap. Mixing the natural mineral with the literature-prepared tetrahedrite sharply increases the thermopower at room temperature, to 179 $\mu V\ K^{-1}$, as zinc is incorporated. These increased thermopower values come as a trade-off for high resistivity, as shown in Figure 4b. The resistivity of the literature-prepared tetrahedrite at room temperature is 7.4 mΩ·cm, or 230% higher than that exhibited by solid-state tetrahedrite (2.2 mΩ·cm). Upon mixing the literature recipe tetrahedrite in a 1:1 molar ratio with natural mineral, we predicted that some metallic behavior would be maintained with 0.9 mol equiv of zinc because the resistivity of tetrahedrite is not reported to rise sharply until after the zinc doping level is increased above the optimum of 1 mol equiv.[2,3] However, the high resistivity of the literature recipe tetrahedrite is further increased by mixing with the natural mineral, to 69 mΩ·cm. This indicates that the Fermi level is raised above the valence band and into the band gap, resulting in a semiconductor or insulator. On the basis of the significant quantities of chlorine detected in the EDS, we attribute this dramatic increase in resistivity to chloride doping in the literature-prepared sample.

Thermal conductivity data for the solid-state tetrahedrite, literature recipe tetrahedrite, and the 1:1 molar mixture of literature recipe tetrahedrite with natural mineral are displayed in Figure 5a. The thermal conductivity at room temperature of the literature recipe tetrahedrite is decreased some 20% from that of the solid-state tetrahedrite (1.3 $W\ m^{-1}\ K^{-1}$) to 1.0 $W\ m^{-1}\ K^{-1}$. The lower thermal conductivity tracks with higher resistivity, and is likely due to decreased electronic contribution to thermal conductivity (κ_C). The thermal conductivity of the 1:1 mole to mole ratio mixture of literature recipe tetrahedrite and tennantite exhibits an even lower thermal conductivity at 0.5 $W\ m^{-1}\ K^{-1}$, again correlating with increasing electronic resistivity.[2,3]

The ZT values are calculated from the thermopower, resistivity, and thermal conductivity values and are displayed in Figure 5b for each of the hot-pressed samples. The literature recipe tetrahedrite exhibits a ZT value of 0.04 at room temperature, a ∼45% decrease from the ZT value of 0.07 calculated for the solid-state tetrahedrite. The sample of literature recipe tetrahedrite mixed in a 1:1 mol to mole ratio with tennantite exhibited an even lower ZT value of 0.03. In spite of higher Seebeck coefficients and lower thermal conductivity values, both samples containing literature tetrahedrite demonstrate lower ZT values than the solid-state tetrahedrite. These decreases must be driven by the increased resistivity values. Compositional impurities, including the chloride doping, clearly increase the resistivity in the literature recipe tetrahedrite disproportionately relative to the small increase achieved in thermopower. On the basis of the poor performance of this material, we elected to not pursue high-temperature ZT measurements and instead focused on developing a chloride-free route to the synthesis of tetrahedrite.

DOI: 10.1021/acsami.5b07141
ACS Appl. Mater. Interfaces 2015, 7, 23623−23632

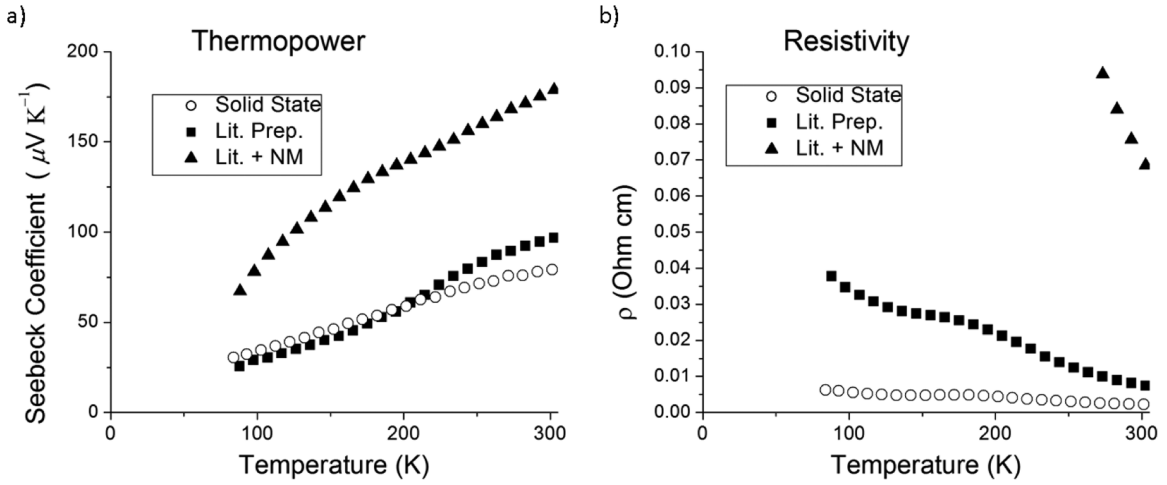

Figure 4. Temperature-dependent Seebeck coefficient (a) and resistivity (b) values are displayed for the hot-pressed samples. These include the solvothermal tetrahedrite prepared by literature methods (Lit. Prep.), the solvothermal tetrahedrite mixed in a 1:1 molar ratio with the natural mineral tennantite, $Cu_{10}Zn_{1.8}Fe_{0.2}As_{2.7}Sb_{1.3}S_{13}$ (Lit. + NM), and the solid-state tetrahedrite (Solid State).

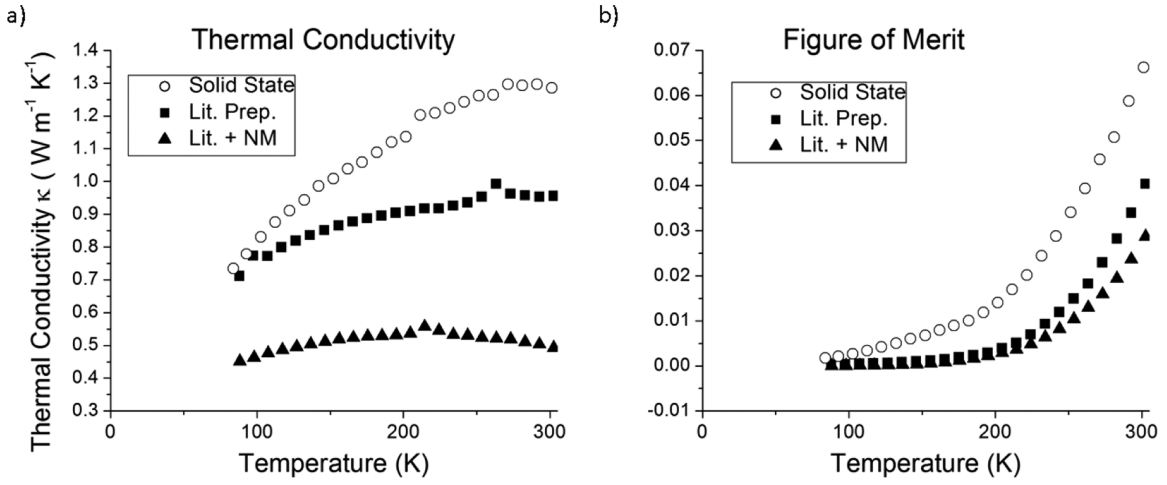

Figure 5. Temperature-dependent thermal conductivity (a) and Figure of Merit, ZT (b) values of the hot-pressed samples. These include the solvothermal tetrahedrite prepared by literature methods (Lit. Prep.), the solvothermal tetrahedrite mixed in a 1:1 molar ratio with the natural mineral tennantite, $Cu_{10}Zn_{1.8}Fe_{0.2}As_{2.7}Sb_{1.3}S_{13}$ (Lit. + NM), and the solid-state tetrahedrite (Solid State).

3.2. Synthesis and Characterization of Tetrahedrite: Optimizing the Solvothermal Synthesis of Tetrahedrite. Because we viewed chloride as a counterion that happens to dope the product, we sought to replace chloride with counterions that would neither act as dopants nor precipitate an insoluble salt with any of the metals present. With this in mind, we decided to avoid not only halogens, but also good Lewis bases such as acetate, oleate, or oleylamine that might leave organic residues that could transform into amorphous carbon during hot-pressing. Nitrate and sulfate were selected as counterions because they are resonance-stabilized conjugate bases of strong acids that are carbon and halogen free, and they do not form insoluble salts with Cu^{+}, Cu^{2+}, or Sb^{3+}. Accordingly, the basic copper nitrate ($Cu_2(OH)_3NO_3$) was chosen as the new source of copper. Antimony nitrate is not commercially available; so, antimony(III) sulfate was used instead.

The reducing solvent ethylenediamine is employed to favor reduction of the Cu^{2+} in the copper source ($Cu_2(OH)_3NO_3$) to Cu^{+}, because 10/12 copper cations present in tetrahedrite are monovalent. To produce a reducing environment, ethylenediamine (en) is reported to complex with the cation Cu^{2+} as $[Cu(en)_3]^{2+}$.[42] Although the copper cation is chelated in this complex, the ligands are constantly exchanging with fresh ethylenediamine from the solvent ($k_{ex} = 1.4 \times 10^7\ s^{-1}$ at 25 °C) by a dissociative-interchange mechanism, leaving Cu^{2+} accessible to nucleophilic attack by the active sulfur source, hydrogen sulfide. The thiourea serves as the source of sulfur by decomposing to form hydrogen sulfide and a water-soluble side product, cyanamide (HNCNH).[43]

To synthesize tetrahedrite, basic copper nitrate ($Cu_2(OH)_3NO_3$) is combined stoichiometrically with antimony(III) sulfate and thiourea in ethylenediamine and heated in a Teflon-lined stainless steel bomb in a furnace at 155 °C for 20−24 h. The product comprises tetrahedrite, chalcostibite ($CuSbS_2$), and antimony(III) oxide (Sb_2O_3) by XRD (Supporting Information, Figure S1). Our early studies indicated that use of excess thiourea could reduce the formation of chalcostibite and Sb_2O_3 (Figure S2), and that crystalline Sb_2O_3 can be removed by sulfuric acid washes in the isolation (Figure S3 for expanded view). The final product (100% excess thiourea and sulfuric acid washes) exhibits the tetrahedrite

DOI: 10.1021/acsami.5b07141
ACS Appl. Mater. Interfaces 2015, 7, 23623−23632

XRD pattern as the major crystalline product, although chalcostibite remains as a significant impurity (Figure 6).

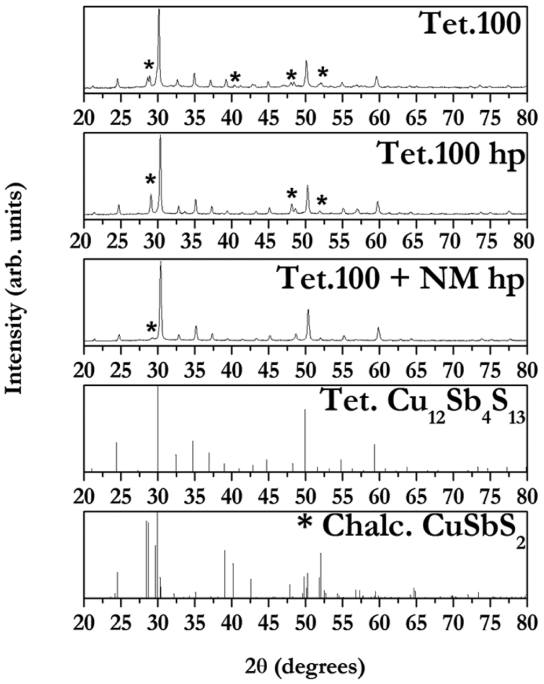

Figure 6. XRD patterns from solvothermal tetrahedrite synthesized with 100% molar excess thiourea (Tet.100) before and after hot-pressing as well as after ball-milling with NM and hot-pressing. Reference patterns for tetrahedrite ($Cu_{12}Sb_4S_{13}$), PDF 42-0561, and chalcostibite ($CuSbS_2$), PDF 44-1417, are displayed below the data plots. The asterisk marks observed peaks due to chalcostibite.

Expanded views of XRD patterns and corresponding metal compositions (determined by ICP-OES) for several repetitions of this synthesis are available in Supporting Information (Figure S4) and also reveal the presence of a small amount of famatinite. The samples are combined in appropriate amounts to obtain a ratio of Sb: Cu of 3.98:12 (scaled to 12 copper) for a formula of $Cu_{12}Sb_{3.98}S_{13}$ (assuming Cu:S is 12:13).

The tetrahedrite peaks as well as the chalcostibite peaks are exhibited before and after hot-pressing the material alone as shown in Figure 6. However, the prevalence of the chalcostibite peaks is greatly decreased by ball-milling the material with the natural mineral before hot-pressing to form a solid solution, due to dilution.

Low-temperature measurements of thermoelectric properties for the chalcostibite-containing samples (Tet.100 hp and Tet.100 + NM hp) are shown in the Supporting Information (Figure S5) and room temperature data comparing materials produced from hot-pressing (with and without NM) solid-state, literature-prepared, and tetrahedrite synthesized with 100% molar excess thiourea are tabulated in the Supporting Information (Table S1). Relative to the literature-prepared material, the resistivity of the Tet.100 hp sample is decreased by over 50%, but that is offset by a decrease in thermopower (20%) and increase in thermal conductivity (20%) resulting in no change in ZT (~45% decreased from the solid-state value). However, in contrast to the literature-prepared material, combining Tet.100 with the NM and hot-pressing increases the ZT. The final value is 2 times that of the similarly processed literature-prepared sample, but still only 30% of what is achieved when the solid-state material is combined with tennantite.

Because the chalcostibite containing tetrahedrite from the solvothermal synthesis performed more poorly than solid-state tetrahedrite, we elected not to pursue high-temperature measurements of ZT and instead endeavored to prevent the formation of the $CuSbS_2$ impurity by further increasing the ratio of sulfur to metal in the reagent mixture. Utilizing a 300% excess of thiourea relative to copper results in a fluctuating composition from batch to batch, as well as a famatinite (Cu_3SbS_4) phase impurity, but suppresses the formation of chalcostibite, $CuSbS_2$ (Supporting Information, Figure S6). The compositions and XRD patterns from several repetitions of this synthesis are displayed in Figure 7. More example compositions of products obtained via this synthesis are available in the Supporting Information (Table S2).

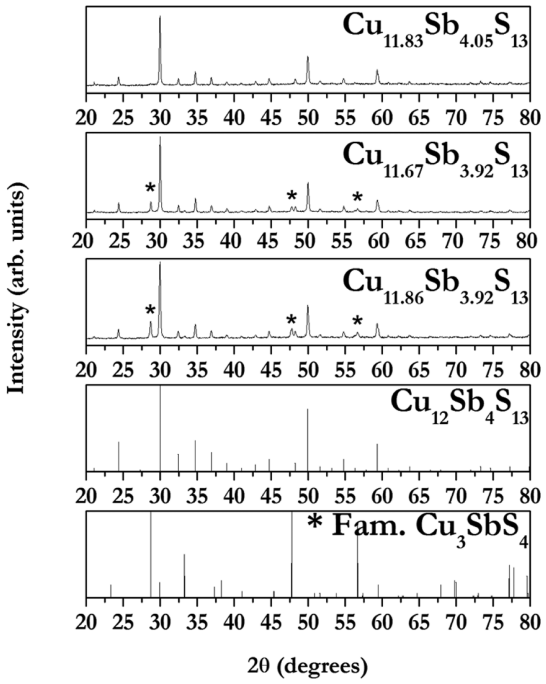

Figure 7. XRD patterns for the tetrahedrite product from several runs of the solvothermal synthesis using 300% molar excess of sulfur precursor. Reference PDF patterns 42-0561 and 35-0581 are displayed for tetrahedrite ($Cu_{12}Sb_4S_{13}$) and famatinite (Cu_3SbS_4), respectively. The ICP-OES determined composition, normalized to $S = 13$, is displayed for each product. The asterisk marks observed peaks for famatinite.

The crystalline famatinite is the likely cause of the fluctuation in composition noticed in this work. To address this fluctuation, the solvothermal products are mixed in appropriate amounts before hot-pressing to achieve an Sb:S atomic ratio of about 4:13 (Supporting Information, Table S2). These solvothermal products tend to be copper poor due to the lower Cu:S ratio in the famatinite impurity. The famatinite crystalline impurity remains after hot-pressing, but the peaks are far less prevalent if the tetrahedrite is mixed with the NM and hot-pressed, again due to dilution (Figure 8).

3.3. Thermoelectric Characterization of Tetrahedrite Prepared with 300% Molar Excess Sulfur. On the basis of previous data from Tet.100 and Tet.100 + NM, and the fact that ZT is maximized for tetrahedrite at high temperatures,

DOI: 10.1021/acsami.5b07141
ACS Appl. Mater. Interfaces 2015, 7, 23623−23632

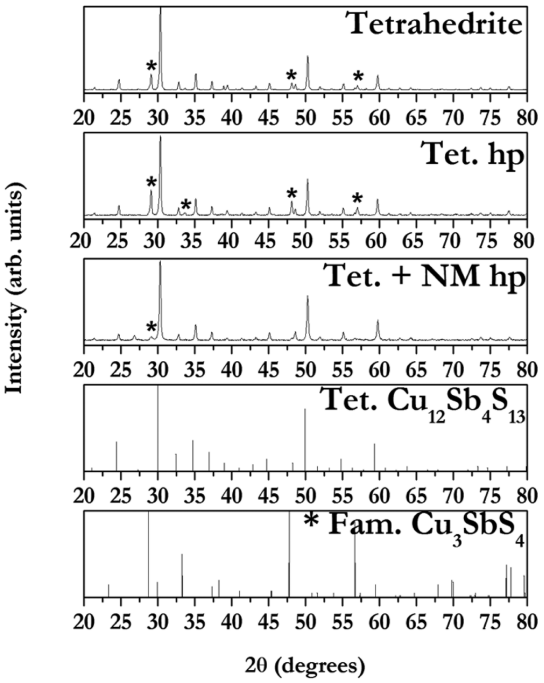

Figure 8. XRD patterns from the solvothermal tetrahedrite synthesized with 300% molar excess thiourea before (Tetrahedrite) and after (Tet. hp) hot-pressing as well as the tetrahedrite ball-milled with NM and hot-pressed (Tet. + NM hp). Reference PDF patterns 42-0561 and 35-0581 are displayed for tetrahedrite ($Cu_{12}Sb_4S_{13}$) and famatinite (Cu_3SbS_4), respectively. The asterisk marks observed peaks for famatinite.

high-temperature (310−730 K) thermoelectric properties were determined for hot-pressed solvothermal tetrahedrite from the 300% molar excess sulfur synthesis with and without mixing of NM. Thermopower values are displayed in Figure 9a. The thermopower curve for the solvothermal tetrahedrite largely overlaps that of the solid-state tetrahedrite. They exhibit similar values at ∼720 K of 130 and 140 μV K^{-1}, respectively. Mixing either the solid-state or solvothermal tetrahedrite with natural mineral tennantite to achieve 0.9 mol equiv of Zn results in a large increase in thermopower across the temperature range. Mixing the solid-state tetrahedrite with NM increases thermopower by ∼40% to 198 μV K^{-1} at ∼720 K. Upon combination with NM, the solvothermal tetrahedrite behaves similarly, increasing thermopower by ∼45% to 202 μV K^{-1}.

Resistivity data are displayed in Figure 9b. The solvothermal tetrahedrite exhibits a similar resistivity curve to that recorded for the solid-state tetrahedrite with a similar value near room temperature and a ca. 20% higher value at ∼720 K (1.9 vs 1.6 mΩ·cm). Mixing NM with the solvothermal tetrahedrite results in a large (∼540%) increase in resistivity at high temperatures, over 2 times that observed for the solid-state material. The rise in resistivity upon combining with NM is attributed to doping by Zn raising the Fermi Level toward the top of the valence band, and thus giving a more semiconductor flavor to the metal.[2,3] Thus, the excessive increase in resistivity in the solovthermal materials may be due to less than optimal Zn doping quantities, as we have not compensated for the material's 4% copper deficiency (Table S2). Alternatively (or additionally), the Famatinite impurities may be playing a role.

The thermal conductivity, κ_{tot}, data for the samples are displayed in Figure 10a. The pure, solid-state tetrahedrite exhibits the highest κ_{tot} across the temperature range. Thermal conductivity for the solvothermal tetrahedrite at the low end (324 K) is 1.2 W m^{-1} K^{-1}, which is close to that of solid-state tetrahedrite, whereas at the high end of the range (∼720 K), there is a ca. 30% decrease in thermal conductivity to 1.0 W m^{-1} K^{-1} from that observed for the solid-state tetrahedrite (1.4 W m^{-1} K^{-1}). Mixing the NM with the solid-state or solvothermal tetrahedrite decreases the thermal conductivity significantly (∼70%) in both samples at the low temperature end (323 K), with a slight positive slope with increasing temperature.

The ZT values as a function of temperature are displayed for each sample in Figure 10b. The solvothermal tetrahedrite performs similarly to the solid-state tetrahedrite over the temperature range studied. This is a large improvement compared to the literature-prepared sample or the Tet.100 sample (ZT = 0.04, at room temperature). Clearly, the higher resistivity and slightly lower thermopower of the solvothermal tetrahedrite compared to solid-state tetrahedrite is effectively compensated for by the decreased thermal conductivity, yielding similar ZT values in the two. Mixing either

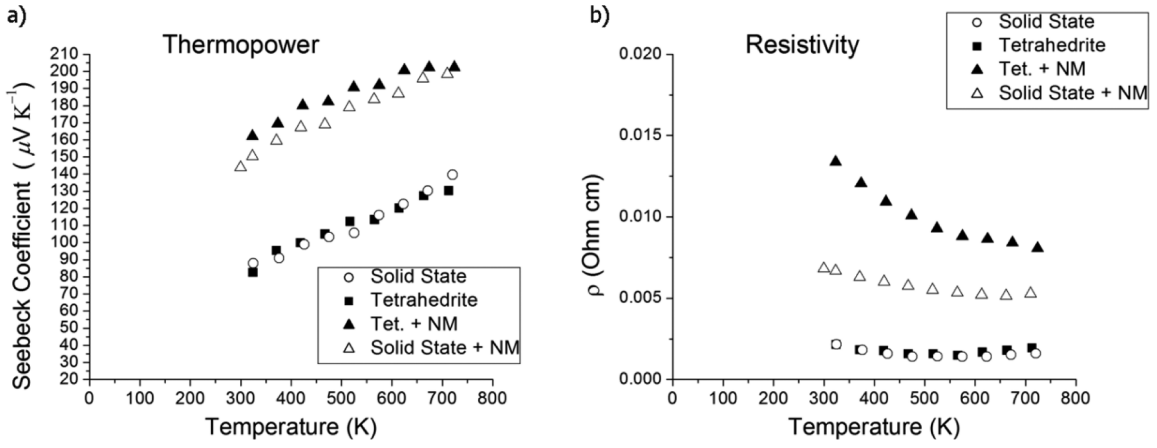

Figure 9. Temperature-dependent Seebeck coefficient (a) and resistivity (b) values from room temperature to 720 K plotted as a function of temperature for the solid-state tetrahedrite (Solid State), the solvothermal tetrahedrite synthesized with 300% molar excess thiourea (Tetrahedrite), the solvothermal tetrahedrite mixed with natural mineral (Tet. + NM), and the solid-state tetrahedrite mixed with NM (Solid State + NM). All samples were hot-pressed.

DOI: 10.1021/acsami.5b07141
ACS Appl. Mater. Interfaces 2015, 7, 23623−23632

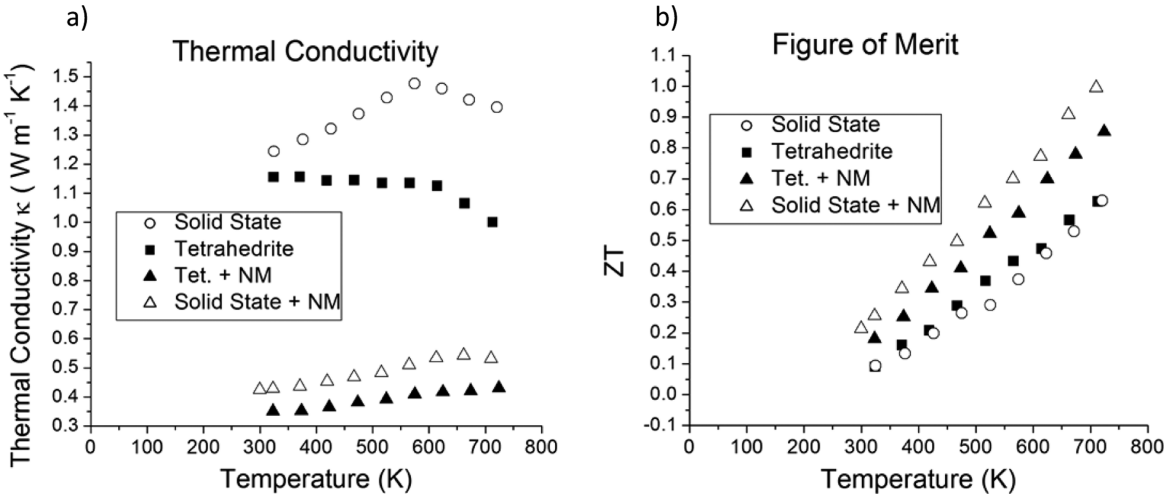

Figure 10. Thermal conductivity (a) and ZT (b) values from room temperature to 720 K plotted as a function of temperature for the solid-state tetrahedrite (Solid State), the solvothermal tetrahedrite synthesized with 300% molar excess thiourea (Tetrahedrite), the solvothermal tetrahedrite mixed with natural mineral (Tet. + NM), and the solid-state tetrahedrite mixed with NM (Solid State + NM).

solvothermal or solid-state tetrahedrite with NM increased ZT values across the temperature range. Near 720 K, the solid-state tetrahedrite and NM mixture reaches unity, a 60% increase over the ZT for the solid-state tetrahedrite alone, whereas the solvothermal tetrahedrite and NM mixture achieves ZT = 0.85 at ~720 K. We expect that the ZT of solovthermal tetrahedrite can be optimized by changing the proportion of NM to optimize the doping and neutralize the effect of famatinite impurities and/or eliminate them entirely.

4. CONCLUSIONS

A chloride-free, solvothermal synthesis of tetrahedrite is developed as a means of quickly and simultaneously producing multiple samples of tetrahedrite at relatively low temperatures (150 °C). The new solvothermal synthesis provides about 0.25 g of tetrahedrite per vessel in a single day and can easily be run in parallel with multiple vessels in an oven, in contrast to solid-state synthetic routes that require higher temperatures and processing that takes 3 days in a furnace, multiple regrindings, and at least 2 weeks of annealing. The use of 100% excess sulfur in the solvothermal synthesis leads to chalcostibite impurities and an unacceptably high resistivity, whereas 300% excess sulfur leads to famatinite impurities that also increase resistivity relative to solid-state materials, but more modestly. Upon mixing the latter with the zinc-rich natural mineral, tennantite, ZT values of 0.85 can be achieved at 720 K, within reach of values obtained with the similarly doped solid-state material. Microstructural analyses are expected to shed further light on the role of impurities in the development of properties in solvothermally prepared tetrahedrite and will be the subject of future investigations.

Current investigations are focused on optimizing the synthesis to further reduce contributions from minor impurity phases and developing in situ doping strategies for inclusion of Zn^{2+} and Mn^{2+} in a single-pot strategy that obviates the need to mix with tennantite. We view the rapid production of "tunable" tetrahedrite as a milestone toward commercialization of thermoelectric devices for widespread application.

■ ASSOCIATED CONTENT

Ⓢ Supporting Information

The Supporting Information is available free of charge on the ACS Publications website at DOI: 10.1021/acsami.5b07141.

XRD patterns of tetrahedrite produced with 300% and 100% molar excess thiourea, before and after hot-pressing alone and with NM; thermoelectric properties for tetrahedrite prepared with 100% molar excess thiourea after hot-pressing alone and with NM (figures). ICP-OES data for differing samples of 300% molar excess-prepared tetrahedrite and their combination to give a near-optimal tetrahedrite composition; near room-temperature thermoelectric properties for the solvothermally prepared and solid-state tetrahedrite samples after hot-pressing alone and with NM (tables) (PDF).

■ AUTHOR INFORMATION

Corresponding Author

*S. L. Brock. E-mail: sbrock@chem.wayne.edu.

Notes

The authors declare no competing financial interest.

§Co-first author

■ ACKNOWLEDGMENTS

This material is based upon work supported as part of the Revolutionary Materials for Solid State Energy Conversion, an Energy Frontier Research Center funded by the U.S. Department of Energy, Office of Science, and Office of Basic Energy Sciences under Award Number DE-SC0001054. Financial support from an A. Paul Schaap Faculty Scholar Award (WSU) is also acknowledged. TEM and HRTEM data were acquired on a JEOL 2010 TEM with funds provided by NSF MRI award 0216084. Structural, elemental characterization and microscopy of materials before hot-pressing were carried out at Wayne State University at the Lumigen Instrument Center (LIC). Assistance from C. Lambert of the LIC with ICP-OES is acknowledged.

DOI: 10.1021/acsami.5b07141
ACS Appl. Mater. Interfaces 2015, 7, 23623−23632

REFERENCES

(1) Shakouri, A. Recent Developments in Semiconductor Thermoelectric Physics and Materials. *Annu. Rev. Mater. Res.* **2011**, *41*, 399−431.

(2) Lu, X.; Morelli, D. T.; Xia, Y.; Zhou, F.; Ozolins, V.; Chi, H.; Zhou, X.; Uher, C. High Performance Thermoelectricity in Earth-Abundant Compounds Based on Natural Mineral Tetrahedrites. *Adv. Energy Mater.* **2013**, *3*, 342−348.

(3) Morelli, D. T.; Lu, X. Natural Mineral Tetrahedrite as a Direct Source of Thermoelectric Materials. *Phys. Chem. Chem. Phys.* **2013**, *15*, 5762−5766.

(4) Ibanez, M.; Zamani, R.; Gorsse, S.; Fan, J.; Ortega, S.; Cadavid, D.; Morante, J. R.; Arbiol, J.; Cabot, A. Core-Shell Nanoparticles as Building Blocks for the Bottom-up Production of Functional Nanocomposites: Pbte-Pbs Thermolectric Properties. *ACS Nano* **2013**, *7*, 2573−2586.

(5) Fang, H.; Luo, Z.; Yang, H.; Wu, Y. The Effects of the Size and Doping Concentration on the Power Factor of N-Type Lead Telluride Nanocrystals for Thermoelectric Energy Conversion. *Nano Lett.* **2014**, *14*, 1153−1157.

(6) Scheele, M.; Oeschler, N.; Veremchuk, I.; Peters, S.; Littig, A.; Kornowski, A.; Klinke, C.; Weller, H. Thermoelectric Properties of Lead Chalcogenide Core-Shell Nanostructures. *ACS Nano* **2011**, *5*, 8541−8551.

(7) Kovalenko, M. V.; Spokoyny, B.; Lee, J.; Scheele, M.; Weber, A.; Perera, S.; Landry, D.; Talapin, D. V. Semiconductor Nanocrystals Functionalized with Antimony Telluride Zintl Ions for Nanostructured Thermoelectric. *J. Am. Chem. Soc.* **2010**, *132*, 6686−6695.

(8) Ganguly, S.; Zhou, C.; Morelli, D.; Sakamoto, J.; Brock, S. L. Synthesis and Characterization of Telluride Aerogels: Effect of Gelation on Thermoelectric Performance of Bi_2te_3 and $Bi_{2-X}sb_xte_3$ Nanostructures. *J. Phys. Chem. C* **2012**, *116*, 17431−17439.

(9) Liang, D.; Yang, H.; Finefrock, S. W.; Wu, Y. Flexible Nanocrystal-Coated Glass Fibers for High-Performance Thermoelectric Energy Harvesting. *Nano Lett.* **2012**, *12*, 2140−2145.

(10) Androulakis, J.; Lin, C. H.; Kong, H. J.; Uher, C.; Wu, C. I.; Hogan, T.; Cook, B. A.; Caillat, T.; Paraskevopoulos, K. M.; Kanatzidis, M. G. Spinodal Decomposition and Nucleation and Growth as a Means to Bulk Nanostructured Thermoelectrics: Enhanced Performance in $Pb_{(1-X)}Sn_{(X)}Te$-Pbs. *J. Am. Chem. Soc.* **2007**, *129*, 9780−9788.

(11) Kishimoto, K.; Koyanagi, T. Preparation of Sintered Degenerate N-Type Pbte with a Small Grain Size and Its Thermoelectric Properties. *J. Appl. Phys.* **2002**, *92*, 2544−2549.

(12) Heremans, J.; Thrush, C.; Morelli, D. Thermopower Enhancement in Lead Telluride Nanostructures. *Phys. Rev. B: Condens. Matter Mater. Phys.* **2004**, *70*, 5−12.

(13) Cao, Y. Q.; Zhu, T. J.; Zhao, X. B. Low Thermal Conductivity and Improved Figure of Merit in Fine-Grained Binary Pbte Thermoelectric Alloys. *J. Phys. D: Appl. Phys.* **2009**, *42*, 015406−015406−6.

(14) Jin, R.; Chen, G.; Pei, J. Pbs/Pbse Hollow Spheres: Solvothermal Synthesis, Growth Mechanism, and Thermoelectric Transport Properties. *J. Phys. Chem. C* **2012**, *116*, 16207−16216.

(15) Mehta, R. J.; Zhang, Y.; Karthik, C.; Singh, B.; Siegel, R. W.; Borca-Tasciuc, T.; Ramanath, G. A New Class of Doped Nanobulk High-Figure-of-Merit Thermoelectrics by Scalable Bottom-up Assembly. *Nat. Mater.* **2012**, *11*, 233−240.

(16) Sumithra, S.; Takas, N.; Nolting, W.; Sapkota, S.; Poudeu, P. P.; Stokes, K. Effect of Nite Nanoinclusions on Thermoelectric Properties of Bi_2Te_3. *J. Electron. Mater.* **2012**, *41*, 1401−1407.

(17) Santhanam, S.; Takas, N. J.; Nolting, W. M.; Poudeu, P. F. P.; Stokes, K. L., Effect of Sn Substitution on the Thermoelectric Properties of Nanostructured Bulk $Bi_{2-X}Sb_xTe_3$ Alloy. *MRS Online Proc.* **2011**, *1329*, DOI: 10.1557/opl.2011.466.

(18) Sumithra, S.; Takas, N. J.; Misra, D. K.; Nolting, W. M.; Poudeu, P. F. P.; Stokes, K. L. Enhancement in Thermoelectric Figure of Merit in Nanostructured Bi_2te_3 with Semimetal Nanoinclusions. *Adv. Energy Mater.* **2011**, *1*, 1141−1147.

(19) Yao, J.; Takas, N. J.; Schliefert, M. L.; Paprocki, D. S.; Blanchard, P. E. R.; Gou, H.; Mar, A.; Exstrom, C. L.; Darveau, S. A.; Poudeu, P. F. P.; Aitken, J. A. Thermoelectric Properties of *P*-Type $CuInSe_2$ Chalcopyrites Enhanced by Introduction of Manganese. *Phys. Rev. B: Condens. Matter Mater. Phys.* **2011**, *84*, 075203−075203−10.

(20) Burnett, J. D.; Gourdon, O.; Ranmohotti, K. G. S.; Takas, N. J.; Djieutedjeu, H.; Poudeu, P. F. P.; Aitken, J. A. Structure−Property Relationships Along the Fe-Substituted $CuInS_2$ Series: Tuning of Thermoelectric and Magnetic Properties. *Mater. Chem. Phys.* **2014**, *147*, 17−27.

(21) Moroz, N. A.; Olvera, A.; Willis, G. M.; Poudeu, P. F. P. Rapid Direct Conversion of $Cu_{2-X}Se$ to Cuagse Nanoplatelets Via Ion Exchange Reactions at Room Temperature. *Nanoscale* **2015**, *7*, 9452−9456.

(22) Lai, W.; Wang, Y.; Morelli, D. T.; Lu, X. From Bonding Asymmetry to Anharmonic Rattling in $Cu_{12}Sb_4S_{13}$ Tetrahedrites: When Lone-Pair Electrons Are Not So Lonely. *Adv. Funct. Mater.* **2015**, *25*, 3648.

(23) Nielsen, M. D.; Ozolins, V.; Heremans, J. P. Lone Pair Electrons Minimize Thermal Conductivity. *Energy Environ. Sci.* **2013**, *6*, 570−578.

(24) Bouyrie, Y.; Candolfi, C.; Pailhes, S.; Koza, M. M.; Malaman, B.; Dauscher, A.; Tobola, J.; Boisron, O.; Saviot, L.; Lenoir, B. From Crystal to Glass-Like Thermal Conductivity in Crystalline Minerals. *Phys. Chem. Chem. Phys.* **2015**, *17*, 19751−19758.

(25) Suekuni, K.; Tomizawa, Y.; Ozaki, T.; Koyano, M. Systematic Study of Electronic and Magnetic Properties for $Cu_{12-X}Tm_xSb_4S_{13}$ (Tm = Mn, Fe, Co, Ni, and Zn) Tetrahedrite. *J. Appl. Phys.* **2014**, *115*, 143702.

(26) Bullett, D. W.; Dawson, W. G. Bonding Relationships in Some Ternary and Quarternary Phosphide and Tetrahedrite Structures: $(Ag_6M_4P_{12})M_6{}'$, $Cu_{12+X}Sb_4S_{13}$ and $Cu_{14-X}Sb_4S_{13}$, $Ln_6Ni_6P_{17}$. *J. Phys. C: Solid State Phys.* **1986**, *19*, 5837.

(27) van Embden, J.; Latham, K.; Duffy, N. W.; Tachibana, Y. Near-Infrared Absorbing $Cu_{12}Sb_4S_{13}$ and Cu_3SbS_4 Nanocrystals: Synthesis, Characterization, and Photoelectrochemistry. *J. Am. Chem. Soc.* **2013**, *135*, 11562−11571.

(28) Heo, J.; Laurita, G.; Muir, S.; Subramanian, M. A.; Keszler, D. A. Enhanced Thermoelectric Performance of Synthetic Tetrahedrites. *Chem. Mater.* **2014**, *26*, 2047−2051.

(29) Makovicky, E.; Forcher, K.; Lottermoser, W.; Amthauer, G. The Role of Fe^{2+} and Fe^{3+} in Synthetic Fe-Substituted Tetrahedrite. *Mineral. Petrol.* **1990**, *43*, 73−81.

(30) Lu, X.; Morelli, D. T.; Xia, Y.; Ozolins, V. Increasing the Thermoelectric Figure of Merit of Tetrahedrites by Co-Doping with Nickel and Zinc. *Chem. Mater.* **2015**, *27*, 408−413.

(31) Lara-Curzio, E.; May, A. F.; Delaire, O.; McGuire, M. A.; Lu, X.; Liu, C.-Y.; Case, E. D.; Morelli, D. T. Low-Temperature Heat Capacity and Localized Vibrational Modes in Natural and Synthetic Tetrahedrites. *J. Appl. Phys.* **2014**, *115*, 193515.

(32) Barbier, T.; Lemoine, P.; Gascoin, S.; Lebedev, O. I.; Kaltzoglou, A.; Vaqueiro, P.; Powell, A. V.; Smith, R. I.; Guilmeau, E. Structural Stability of the Synthetic Thermoelectric Ternary and Nickel-Substituted Tetrahedrite Phases. *J. Alloys Compd.* **2015**, *634*, 253−262.

(33) Chetty, R.; D. S., P. K.; Rogl, G.; Rogl, P.; Bauer, E.; Michor, H.; Suwas, S.; Puchegger, S.; Giester, G.; Mallik, R. C. Thermoelectric Properties of a Mn Substituted Synthetic Tetrahedrite. *Phys. Chem. Chem. Phys.* **2015**, *17*, 1716−1727.

(34) Momma, K.; Izumi, F. Vesta 3 for Three-Dimensional Visualization of Crystal, Volumetric and Morphology Data. *J. Appl. Crystallogr.* **2011**, *44*, 1272−1276.

(35) Morelli, D. T.; Lu, X.; Ozolins, V. Thermoelectric Materials Based on Tetrahedrite Structure for Thermoelectric Devices. Patent WO2014008414A1, January 9, 2014.

(36) Morelli, D. T.; Lu, X. Thermoelectric Materials Based on Tetrahedrite Structure for Thermoelectric Devices. Patent WO2015003157A1, January 8, 2015.

(37) Ramasamy, K.; Sims, H.; Butler, W. H.; Gupta, A. Selective Nanocrystal Synthesis and Calculated Electronic Structure of All Four

DOI: 10.1021/acsami.5b07141
ACS Appl. Mater. Interfaces 2015, 7, 23623−23632

Phases of Copper−Antimony−Sulfide. *Chem. Mater.* **2014**, *26*, 2891−2899.
(38) Talapin, D. V.; Murray, C. B. Pbse Nanocrystal Solids for N- and P-Channel Thin Film Field-Effect Transistors. *Science* **2005**, *310*, 86−89.
(39) Urban, J. J.; Talapin, D. V.; Shevchenko, E. V.; Kagan, C. R.; Murray, C. B. Synergism in Binary Nanocrystal Superlattices Leads to Enhanced P-Type Conductivity in Self-Assembled PbTe/Ag_2Te Thin Films. *Nat. Mater.* **2007**, *6*, 115−121.
(40) Liu, Y.; Sahoo, P.; Makongo, J. P. A.; Zhou, X.; Kim, S.-J.; Chi, H.; Uher, C.; Pan, X.; Poudeu, P. F. P. Large Enhancements of Thermopower and Carrier Mobility in Quantum Dot Engineered Bulk Semiconductors. *J. Am. Chem. Soc.* **2013**, *135*, 7486−7495.
(41) An, C.; Jin, Y.; Tang, K.; Qian, Y. Selective Synthesis and Characterization of Famatinite Nanofibers and Tetrahedride Nanoflakes. *J. Mater. Chem.* **2003**, *13*, 301−303.
(42) Inada, Y.; Ozutsumi, K.; Funahashi, S.; Soyama, S.; Kawashima, T.; Tanaka, M. Structure of Copper(II) Ethylenediamine Complexes in Aqueous and Neat Ethylenediamine Solutions and Solvent-Exchange Kinetics of the Copper(II) Ion in Ethylenediamine as Studied by EXAFS and NMR Methods. *Inorg. Chem.* **1993**, *32*, 3010−3014.
(43) Wang, Z. D.; Yoshida, M.; George, B. Theoretical Study on the Thermal Decomposition of Thiourea. *Comput. Theor. Chem.* **2013**, *1017*, 91−98.

DOI: 10.1021/acsami.5b07141
ACS Appl. Mater. Interfaces 2015, 7, 23623−23632